Ca^{2+} binding by domain 2 plays a critical role in the activation and stabilization of gelsolin

Shalini Nag[a,1], Qing Ma[a,b,1], Hui Wang[c,1], Sakesit Chumnarnsilpa[a], Wei Lin Lee[a], Mårten Larsson[a], Balakrishnan Kannan[a], Maria Hernandez-Valladares[a], Leslie D. Burtnick[c], and Robert C. Robinson[a,2]

[a]Institute of Molecular and Cell Biology, A*STAR, 61 Biopolis Drive, Proteos, Singapore 138673; [b]Institutionen för Medicinsk Biokemi och Mikrobiologi, Box 582, 751 23 Uppsala, Sweden; and [c]Department of Chemistry and Centre for Blood Research, Life Sciences Institute, University of British Columbia, Vancouver, BC, Canada V6T 1Z1

Edited by Thomas D. Pollard, Yale University, New Haven, CT, and approved July 7, 2009 (received for review December 8, 2008)

Gelsolin consists of six homologous domains (G1–G6), each containing a conserved Ca-binding site. Occupation of a subset of these sites enables gelsolin to sever and cap actin filaments in a Ca-dependent manner. Here, we present the structures of Ca-free human gelsolin and of Ca-bound human G1–G3 in a complex with actin. These structures closely resemble those determined previously for equine gelsolin. However, the G2 Ca-binding site is occupied in the human G1–G3/actin structure, whereas it is vacant in the equine version. In-depth comparison of the Ca-free and Ca-activated, actin-bound human gelsolin structures suggests G2 and G6 to be cooperative in binding Ca^{2+} and responsible for opening the G2–G6 latch to expose the F-actin-binding site on G2. Mutational analysis of the G2 and G6 Ca-binding sites demonstrates their interdependence in maintaining the compact structure in the absence of calcium. Examination of Ca binding by G2 in human G1–G3/actin reveals that the Ca^{2+} locks the G2–G3 interface. Thermal denaturation studies of G2–G3 indicate that Ca binding stabilizes this fragment, driving it into the active conformation. The G2 Ca-binding site is mutated in gelsolin from familial amyloidosis (Finnish-type) patients. This disease initially proceeds through protease cleavage of G2, ultimately to produce a fragment that forms amyloid fibrils. The data presented here support a mechanism whereby the loss of Ca binding by G2 prolongs the lifetime of partially activated, intermediate conformations in which the protease cleavage site is exposed.

actin | calcium activated | calcium dependent | TIRF

Gelsolin is a calcium-dependent, multifunctional regulator of actin filament dynamics (1). It is present in a wide range of cell types and exists in extracellular (83 kDa) and cytoplasmic (81 kDa) forms that are generated from the same gene by initiation of transcription at alternative sites and selective processing of RNA (2–5). In the Ca-free, inactive form of equine gelsolin, the six similarly folded domains (G1–G6) adopt a compact globular structure held together by extensive noncovalent interactions of G2 with both G6 and the C-terminal tail (C-terminal latch), such that the actin-binding sites in G1, G2, and G4 are buried (6).

Sequence and structural data (7–10) suggest that activated actin-bound gelsolin has eight Ca-binding sites. Two, associated with G1 and G4, are identified as type 1, with the metal ion coordinated by residues from both actin and gelsolin (7). Six—one in each domain—are type 2, with the cation coordinated by residues from gelsolin alone (7). Surprisingly, then, the crystal structure of equine G1–G3 in a complex with actin (9) shows the type 2 site in G2 to be incompletely formed and devoid of Ca^{2+}. That this locale within G2 can be induced to form a valid metal ion-binding site is verified by the ability of Tb^{3+} ions to soak into crystals of the complex of equine G1–G3 with actin and occupy the site (8). Furthermore, a Cd^{2+} is found in the structure of isolated human G2, coordinated by the side chains of Asp-187, Glu-209, and Asp-259 (10). In isolated G2, differential scanning calorimetry reveals a 16.5 °C increase in T_m, supporting the hypothesis, based on molecular dynamics simulation data, that Ca^{2+} stabilizes the fragment (10).

Ca binding disrupts the interactions between G2 and G6, releases the C-terminal latch, and induces large interdomain rearrangements that result in activation (7, 9, 11, 12). During this process, domains G3 and G6 undergo rotations of ≈90° and translations of ≈40 Å relative to G1 and G4, respectively, and they form new contacts with G2 and G5, respectively (7, 9). The latch mechanism for Ca-induced activation is supported by studies that show that although G1–G3 in isolation function in a Ca-independent manner (13), G4–G6 must bind Ca^{2+} in two high-affinity sites to bind actin (14). Various biophysical approaches provide insight into the conformational changes induced by Ca binding. Dynamic light scattering experiments demonstrate the hydrodynamic radius of gelsolin to increase from 3.9 to 4.5 nm upon binding Ca^{2+} in solution (15, 16). This can be reversed by addition of EGTA to chelate free Ca^{2+}, and it is consistent with domain reorganization evident in various crystalline forms of the protein (6, 7, 9). Radiolytic footprinting and small-angle X-ray scattering experiments concur that the structural activation of gelsolin is a two-step, three-state process. The first shift, from the inactive to an intermediate state, occurs at ≈0.1 to ≈5 μM Ca^{2+}. The second, to the activated state, occurs at ≈10 μM to 1 mM Ca^{2+} (17–19).

A single mutation within the type 2 metal ion-binding site in G2—of Asp-187 to Asn or Tyr—is the cause of familial amyloidosis Finnish-type (FAF), characterized by the extracellular deposition of a 71-residue fragment of gelsolin (20). It has been proposed that this mutation destabilizes gelsolin through loss of Ca coordination at the type 2 site in G2 (10), making it susceptible to cleavage by furin in the acidic *trans*-Golgi compartment (21). The resulting 68-kDa fragment is further cleaved by membrane-associated type I matrix metalloproteases located proximal to the extracellular matrix (22) into 8- and 5-kDa fragments, Ala-173-Met-243 and Ala-173-Arg-225, respectively, which form the deposits (20, 23). Aggregation assays demonstrate that wild-type gelsolin Ala-173-Met-243 is as amyloidogenic as the corresponding fragment containing the Asp187Asn mutation and is more amyloidogenic than the one containing the Asp187Tyr mutation. Therefore, although the mutation enables

Author contributions: M.H.-V., L.D.B., and R.C.R. designed research; S.N., Q.M., H.W., S.C., W.L.L., M.L., and B.K. performed research; S.N., Q.M., W.L.L., M.L., and B.K. analyzed data; and S.N., L.D.B., and R.C.R. wrote the paper.

The authors declare no conflict of interest.

This article is a PNAS Direct Submission.

Freely available online through the PNAS open access option.

Data deposition: The coordinates for Ca-free recombinant human gelsolin and for Ca-bound recombinant human G1–G3 bound to native rabbit actin have been deposited with the RCSB (RCSB ID codes 3FFN and 3FFK, respectively).

[1]S.N., Q.M., and H.W. contributed equally to this work.

[2]To whom correspondence should be addressed. E-mail: rrobinson@imcb.a-star.edu.sg.

This article contains supporting information online at www.pnas.org/cgi/content/full/0812374106/DCSupplemental.

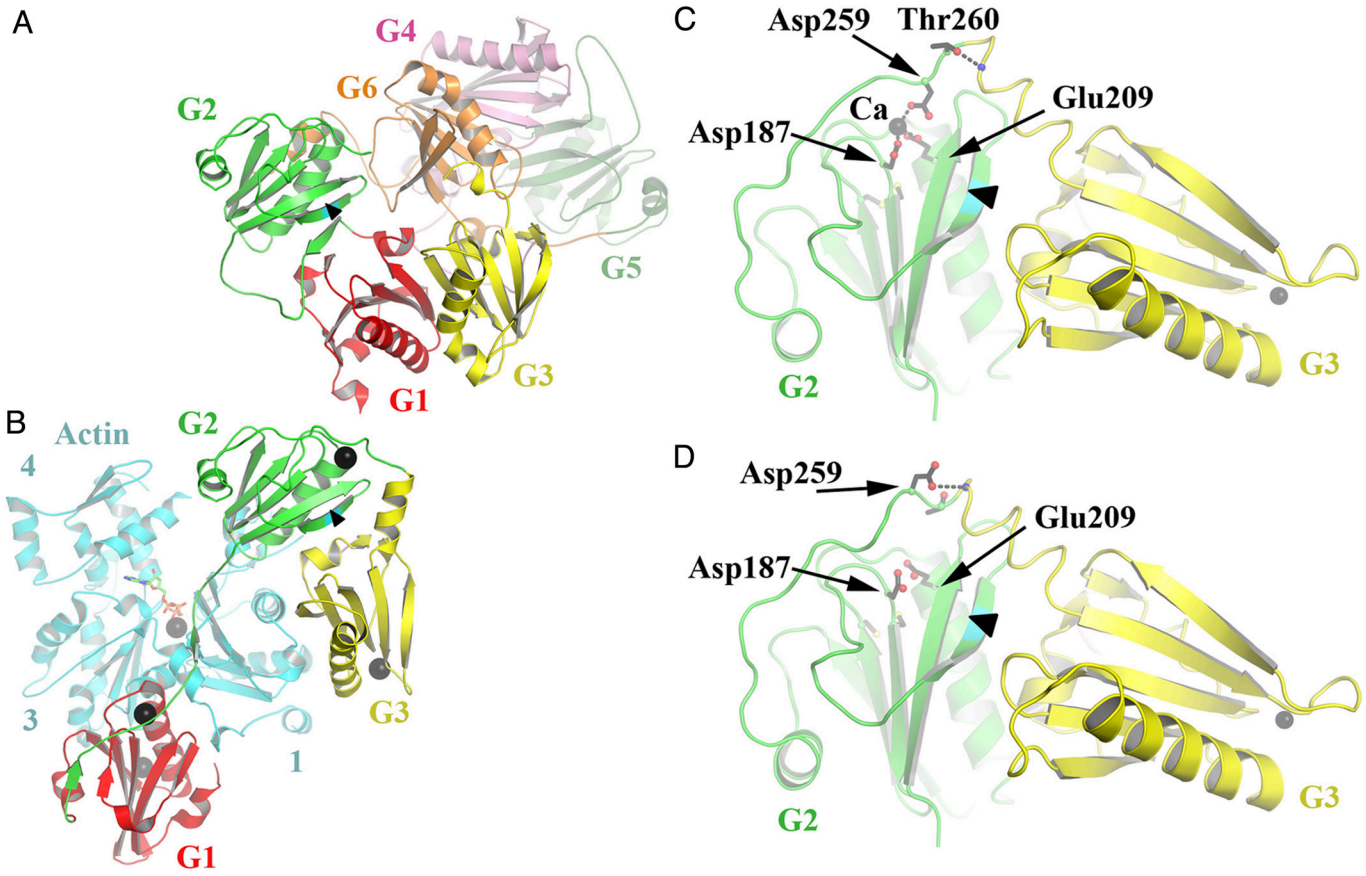

Fig. 1. Structures of Ca-free human gelsolin and human G1–G3/actin. (*A*) Schematic representation of the structure of Ca-free human gelsolin. The arrowhead in this part, as in the others, points toward the peptide bond between Arg-172 and Ala-173, which gets cleaved in FAF. (*B*) The structure of human G1–G3 bound to actin. G2 is shown in a similar orientation as in *A*. There are five Ca^{2+} ions (black spheres) associated with this structure, one bound to each gelsolin domain, another sandwiched between G1 and actin, and one at the ATP-binding site of actin. (*C*) Close up of the Ca-coordinating residues in G2 from human G1–G3/actin. Only G2–G3 is shown for clarity. (*D*) Close up of the vacant G2 Ca-binding site from equine G1–G3/actin (Protein Data Bank ID 1RGI). Protein representations were generated here and in the figures that follow by using PYMOL (http://pymol.sourceforge.net/).

aberrant furin cleavage, it does not confer additional amyloidogenicity (24).

In this report, we present the structures of Ca-free inactive human gelsolin and Ca-bound human G1–G3 in complex with actin. Not surprisingly, they closely resemble their equine gelsolin counterparts (6, 9). However, Ca-free human gelsolin lacks the disulfide bond between Cys-188 and Cys-201 that is found in Ca-free equine gelsolin. More interestingly, a Ca^{2+} is clearly present in the G2 type 2 metal ion site in the complex of human G1–G3 with actin, whereas it is absent in the corresponding equine structure. This observation prompted us to probe the role of G2 type 2 metal binding in the mechanism for release of the C-terminal latch in inactive gelsolin by comparing thermal stabilities and F-actin depolymerization activities of wild-type gelsolin with those of two engineered variants, one lacking the C-terminal helix and another in which acidic side-chain residues in the type 2 sites of G2 and G6 are mutated. We propose that cooperative binding of the Ca^{2+} in these sites in G2 and G6 is a critical step in releasing the C-terminal latch and initiates the large-scale conformational changes required for activation. We also put forward a mechanism for the furin-induced cleavage of gelsolin in subjects carrying the FAF mutation.

Results and Discussion

Human Gelsolin Structures. The structure of recombinant, Ca-free human gelsolin was determined at 3-Å resolution. It is almost identical to that of Ca-free equine gelsolin (6), except that the disulfide bridge between Cys-188 and Cys-201 is absent. Domains G1–G5 are arranged in a compact fashion around the central domain, G6 (Figs. 1*A* and 2*A*), with the result that all actin-binding surfaces, both major (G1, G2, and G4) and minor (G3 and G6), are obscured. The structure of recombinant human G1–G3 bound to actin in the presence of Ca^{2+} was also resolved at 3 Å. It revealed the same large-scale rearrangement of domains G1 and G3 relative to G2 that are required in equine G1–G3 for binding actin (9) (Fig. 1*B*, compare with *A*). Rupture of the central β-sheet that runs through both G1 and G3 and removal of the first strand from the β-sheet in G2 expose actin-binding interfaces and create a new G2–G3 interface. This structure differs from that of equine G1–G3/actin in three aspects. First, there is a disulfide bridge between Cys-188 and Cys-201, which is absent in the corresponding equine G1–G3 structure (9). Second, the human G1–G3/actin complex contains five bound Ca^{2+}, whereas only four are present in equine G1–G3/actin (9). The additional Ca^{2+} is located in the G2 type 2 metal ion site. Finally, inspection of this particular type 2 site reveals that Asp-259, from the G2–G3 linker (Fig. 1*C*), completes the Ca-coordination sphere, together with other conserved type 2 site residues (Asp-187 and Glu-209), as observed in the structure of isolated human G2 with a bound Cd^{2+} (10). This positions the G2–G3 linker such that Thr-260 forms a helix-initiating hydrogen bond that contributes to the contraction of the previously disordered G2–G3 linker into a helix to allow close packing of G3 with G2. In contrast, in equine

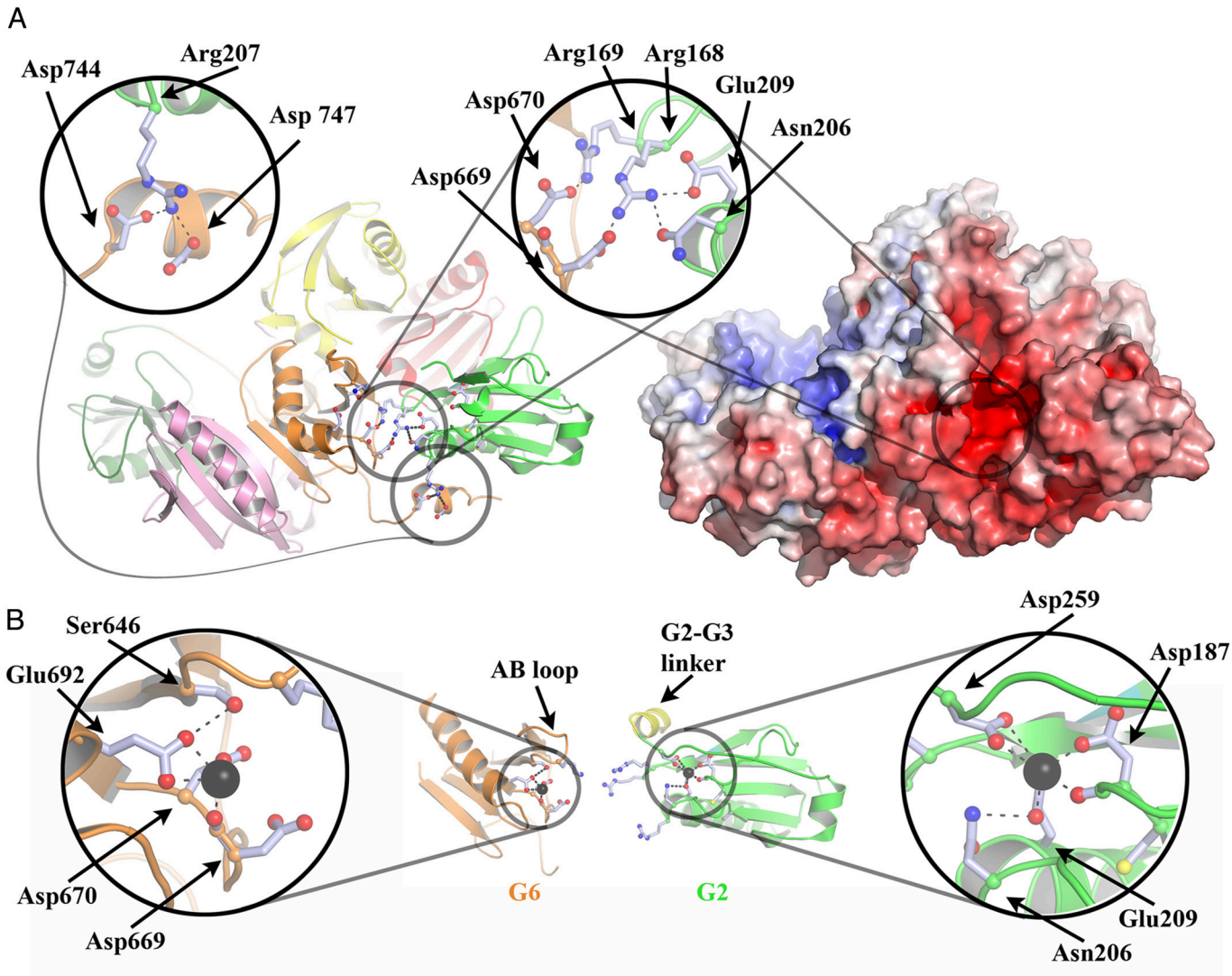

Fig. 2. Structural interdependence of the G2 and G6 Ca-binding sites. (*A*) Schematic and electrostatic surface representations of Ca-free human gelsolin, highlighting the charged residues at the G2–G6 interface. (*B*) Schematic representations of Ca-bound G6 and G2, taken from the structures of Ca-bound equine G4–G6/actin (Protein Data Bank ID 1H1V) and human G1–G3/actin, respectively, in orientations similar to those presented in *A*. G2 and G6 have been translated relative to their positions in *A* to avoid steric clashes. Note that the Ca ions are coordinated by residues that previously made up the network of interactions between G2 and G6 in *A*.

G1–G3/actin, Asp-259 is not bound to Ca^{2+} and itself becomes the helix-initiating residue, allowing the linker to condense to bring G2 and G3 together (Fig. 1*D*) (9).

G2 and G6 Ca-Binding Sites in Ca-Free Gelsolin. Examination of the electrostatic surface of Ca-free human gelsolin reveals two distinctive charged patches: a highly positively charged patch that is the polyphosphate-binding site for ATP and is speculated to bind PIP_2 (25), and a highly negatively charged patch at the junction of G2 and G6 that encompasses the two unoccupied type 2 Ca-binding sites (Fig. 2*A*). Residues from both vacant Ca-binding sites participate in complex electrostatic interactions at the G2–G6 interface. In particular, Arg-168 and Arg-169 interact directly with Asp-669 and Asp-670, respectively, from the G6 Ca-binding site, whereas Arg-168 also binds to Glu-209 and Asn-206 in the G2 Ca-binding site. Further interactions linking Asp-744 and Asp-747 to Arg-207 tether the tail across the F-actin-binding site on G2. Hence, binding of Ca^{2+} to these sites is likely to be interdependent and cooperative with regard to breaking the G2–G6 interface.

Ca-Bound G2 and G6. Ca binding by G2 has a number of consequences (Fig. 2*B*). To coordinate Ca^{2+}, Glu-209 releases Arg-168 and moves closer to Asp-187, taking Asn-206 with it. This leads to mobility in Arg-168 and, through proximity, in Arg-169, weakening the G2–G6 contact. The slight straightening of the G2 long helix, to which Asn-206 and Glu-209 are attached, alters the position of Arg-207. Because Arg-207 interacts directly with the C-terminal tail, Ca binding by G2 is likely to be a factor in releasing the tail during activation. Furthermore, participation of Asp-259 in Ca coordination by G2 promotes order in the previously disordered G2–G3 linker. This introduces a steric element into the activation process, because an ordered G2–G3 linker is incompatible with the position of G6 in the inactive structure. Thus, Ca binding by G2 potentially has a 3-fold effect on the initial activation of gelsolin via altering contacts with the C-terminal tail, disordering the G2–G6 interface, and promoting a conformational state in the G2–G3 linker that is incompatible for association with G6.

Similarly, Ca binding by G6 has a direct effect on the G2–G6 interface. The side chains of Asp-669 and Asp-670 lock the

G2–G6 interface through binding to Arg-168 and Arg-169, respectively. Direct competition by Ca^{2+} for the Asp-670 side chain and conformational restriction of Asp-669 through coordination by its carboxylate destabilize the G2–G6 interface. Furthermore, the straightening of the long helix of G6, required for the constitution of a functional Ca-binding site, is achieved by the movement of the AB loop of G6 through formation of a hydrogen bond between Ser-646 (from the AB loop) and Glu-692 (from the Ca-coordination sphere) (Fig. 2*B*). The activated conformation of the G6 AB loop causes a steric clash with G2, and is therefore incompatible with Ca-free gelsolin. Thus, Ca binding to G2 and G6 directly competes for residues involved in the G2–G6 interface and induces conformational changes in both domains, rendering them incompatible with the Ca-free structure.

The structure of Ca-free gelsolin strongly suggests that the vacant type 2 Ca-binding sites in G2 and G6: (*i*) are available; (*ii*) are set in an electrostatic environment that attracts cations; (*iii*) bind cooperatively to Ca^{2+}; and (*iv*) support local conformational rearrangements appropriate for springing the G2–G6 latch. It has been proposed that the disulfide in G2 is involved in Ca activation of gelsolin (26). In our structure of G1–G3/actin, both the disulfide bond and a Ca^{2+} bound to the G2 Ca-binding site are present. Juxtaposition of the disulfide-forming residue, Cys-188, and Ca-binding residue, Asp-187, offers an explanation for the reported influence of the disulfide bond on the affinity of this site for Ca^{2+}.

Mutation of G2 and G6 Ca-Binding Sites. Residues in the Ca-binding sites of G2 and G6 play multiple roles in regulating gelsolin structure: stabilizing the Ca-free state, driving gelsolin through intermediate states, and stabilizing the Ca-bound state. Hence, mutational analysis presents a challenging task in separating contributions to each state. Here, we chose to mutate, in each site, the two conserved Ca-coordinating residues Asp and Glu to Asn and Gln, respectively. This mirrors the Asp187Asn mutation observed in FAF by replacing a single oxygen atom with a nitrogen atom in each mutation.

Depolymerization of F-actin in the presence EGTA was monitored by the loss of fluorescence of pyrene-labeled F-actin in the presence of the gelsolin mutants (Fig. 3*A*). Single mutations in the Ca-binding site of G2, Asp187Asn (D2), or Glu209Gln (E2); or of G6, Asp670Asn (D6), or Glu692Gln (E6), as well as combinations of double mutations for each site or between sites, showed wild-type gelsolin (GFL) behavior in not being able to depolymerize actin in the absence of Ca. Triple mutants D2E2D6 and D2D6E6 showed significant levels of depolymerizing activity, whereas the quadruple mutant D2E2D6E6 displayed even greater activity. These data demonstrate that mutations within a single site do not engender activity. However, cooperativity between sites leads to activation. A truncated gelsolin (GTL), which lacks part of the tail latch (residues 742–755) and is equivalent to the length of adseverin, showed slightly greater activity than the quadruple mutant. All mutants displayed increased depolymerization kinetics, similar to wild type, in the presence of 10 μM Ca (Fig. 3*B*), confirming the conservative nature of the mutations. The effects of GTL and the quadruple mutant on fluorescently labeled F-actin in EGTA were observed by total internal reflection fluorescence (TIRF) microscopy. Under conditions that show no activity for GFL (ratio to actin, 1:200), both GTL and the quadruple mutant were observed to sever (Fig. 3 *E–G* and Movies S1–S3).

The activity of GTL and the quadruple mutant in the absence of Ca suggests that both mutants destabilize the C-terminal latch. GTL has part of the latch deleted, whereas the quadruple mutant is predicted to destabilize the G2–G6 interface, either through loss of stabilizing interactions or by partial mimicking of Ca binding due to the charge reversal in the mutated Ca-binding

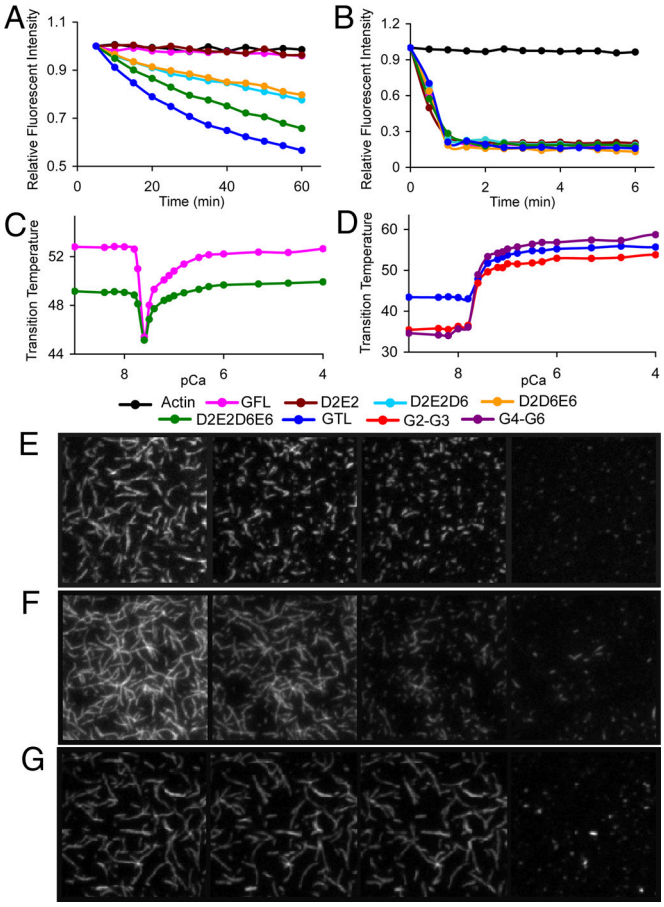

Fig. 3. Ca effects on gelsolin structure and function. (*A* and *B*) Actin depolymerization assays. A total of 6 μM of each protein was added to 12 μM F actin in the presence of (*A*) 1 mM EGTA and (*B*) 10 μM free Ca^{2+}. Single mutants (D2, E2, D6, and E6) and double mutants (D2D6, D2E6, E2D6, E2E6, and D6E6) were indistinguishable from GFL and are not shown for clarity. TIRF analysis confirmed that gelsolin severs actin under these conditions (Movie S4). (*C* and *D*) Thermal shift assays. (*C*) Effect of Ca concentration on thermal stability of GFL and the D2E2D6E6 quadruple mutant. (*D*) Effect of Ca concentration on thermal stability of GTL, G2–G3, and G4–G6. pCa refers to the theoretical free Ca concentration that is not bound to EGTA in the absence of protein. (*E–G*) TIRF assay. TIRF images of actin filaments (500 nM) severed by (*E*) GTL (2.5 nM), (*F*) D2E2D6E6 (2.5 nM), and (*G*) GFL (2.5 nM) in 1 mM EGTA buffer. Shown are 40 × 40 μm snapshots at four different time points (from left to right): (*E*) before mixing and 40 s, 80 s, and 17.5 min after mixing; (*F*) before mixing and 2, 4, and 17.5 min after mixing; and (*G*) before mixing, 140 s after mixing, 4 mins after mixing, and 35 s after adding Ca^{2+} (5 mM) to the stable mixture. Movies of *E*, *F*, and *G* and a description of the TIRF experiment are available in the *SI Text* and Movies S1–S3.

sites. The activity of the quadruple mutant implies that a number of the eight gelsolin Ca-binding sites are not needed for minimal levels of activity. The existence of apparently dispensable Ca-binding sites can be justified by their possible effects on the rate of gelsolin action, achieved through stabilization of an optimal conformation and direct mediation of contact with actin at higher Ca^{2+} concentrations. Thus, gelsolin is able to respond to the four orders of magnitude of variation in Ca^{2+} levels found between intracellular and extracellular environments.

To further determine the integrity and properties of the mutants, we undertook thermal shift assays as a function of Ca concentration. These assays use a fluorescent hydrophobic dye to monitor the temperature-induced unfolding of gelsolin, and the data are plotted as the midpoints of the unfolding transition (T_m). GFL displays a Ca-induced destabilization followed by

restabilization in this assay (Fig. 3*C*). In contrast, fragments of gelsolin, G2–G3, and G4–G6 demonstrate only stabilization within this range of Ca^{2+} concentrations (Fig. 3*D*), suggesting that G2–G3 and G4–G6 adopt stable compact structures on binding Ca^{2+}, in line with their Ca-bound structural data. Unfortunately, G1–G3 precipitated in the absence of Ca^{2+}, so a similar titration could not be performed. The initial loss in thermal stability of GFL can be rationalized by the Ca-triggered opening of the C-terminal latch to achieve a state of reduced thermal stability. The Ca^{2+} levels at which gelsolin, G2–G3, and G4–G6 undergo their respective transitions are indistinguishable. However, the Ca concentrations of the transitions are not physiologically meaningful because of the temperature dependence of gelsolin interactions with Ca (27) and the limited Ca-buffering capacity of the EGTA solutions. GTL was less thermally stable than GFL in the absence of Ca and showed a shift to higher stability on binding Ca (Fig. 3*D*). This suggests that the release of the tail during Ca activation in GFL is responsible for the initial loss in the thermal stabilization (Fig. 3*C*). The quadruple mutant (D2E2D6E6) displayed a profile similar to that of wild-type gelsolin, with the exception that the Ca-free and Ca-bound states displayed relatively lower thermal stability. This profile is consistent with the notion that the mutations may partially mimic Ca binding at these sites, but it also infers that a further Ca-binding event is needed to fully open the C-terminal latch.

Loss of G2 Ca Binding in FAF. The importance of the G2 Ca-binding site in the activation of gelsolin and the presence of a Ca^{2+} at this site in the human G1–G3/actin structure have implications for FAF. In this heritable disease, Asp-187, which is part of the G2 Ca-coordination sphere, is mutated to Asn or Tyr (20). The mutant proteins are unable to bind Ca^{2+} at this site and can be predicted to have three abnormalities with regard to Ca-dependent activation. First, the initial opening of the G2–G6 latch is compromised because of a lack of the Ca-induced conformational changes in G2 and the loss of cooperativity with the G6 Ca-binding site, although this has little effect on overall activity in vitro (Fig. 3 *A* and *B*). Second, Ca-induced stabilization of the G2–G3 module in the activated conformation will be absent (Fig. 3*D*). Finally, should the mutant gelsolin be able to become fully activated, the final conformation of G2–G3 would resemble that observed in the equine structure (Fig. 1*D*), rather than in the human structure (Fig. 1*C*). The first step in the progression of the disease is the furin cleavage of G2 between Arg-172 and Ala-173 (21). This peptide bond is protected in inactive gelsolin by the flanking strands within the core β-sheet of G2 (Fig. 1*A*) (6). In the activated conformation, the peptide bond is protected by G3, even in the absence of G2-bound Ca^{2+} (Fig. 1*D*) (9). However, in intermediate conformations, where G1 has dissociated from G2 but G3 has yet to bind to G2 (at any stage between those depicted in Fig. 1 *A* and *B*), the cleavage site is accessible to the protease. Ca binding drives G2–G3 into its stable active conformation (Figs. 1*C* and 3*D*), minimizing the time spent in the intermediate states and reducing the window of opportunity for cleavage by furin, which would set gelsolin on a course to fibril formation. Hence, we propose that the protease cleaves gelsolin during the activation process, when Arg-172 and Ala-173 become exposed, and that Ca binding to G2 in wild-type gelsolin protects it from furin and prevents FAF by enhancing the rate of activation.

Materials and Methods

Constructs. Recombinant full-length human cytoplasmic gelsolin (GFL) residues 25–755 (accession number P06396, numbering based on plasma gelsolin) and fragments G1–G3 (residues 25–372) and G2–G3 (residues 132–372) were engineered into the expression vector pSY5, a modified version of pET-21d(+) (Novagen), encoding an N-terminal, eight-histidine tag, followed by a human rhino-virus 3C protease cleavage site ahead of the N terminus of the proteins. Gelsolin fragment G4–G6 (residues 414–742) was described previously (12). Mutated variants of GFL [single mutants: Asp187Asn (D2), Glu209Gln (E2), Asp670Asn (D6), and Glu692Gln (E6); double mutants: Asp187Asn Asp670Asn (D2D6), Asp187Asn Glu692Gln (D2E6), Glu209Gln Asp670Asn (E2D6), Glu209Gln Glu692Gln (E2E6), Asp187Asn Glu209Gln (D2E2), and Asp670Asn Glu692Gln (D6E6); triple mutants: Asp187Asn Glu209Gln Asp670Asn (D2E2D6) and Asp187Asn Asp670Asn Glu692Gln (D2D6E6); and quadruple mutant: Asp187Asn Glu209Gln Asp670Asn Glu692Gln (D2E2D6E6)] as well as tailless gelsolin (GTL) residues 25–741 were constructed by using a QuikChange site-directed mutagenesis kit (Stratagene) with the full-length wild-type gelsolin as the template. DNA sequencing using an Applied Biosystems ABI Prism 373 Genetic Analyzer verified the identities of the constructs.

Protein Production. Recombinant proteins were expressed in *Escherichia coli* Rosetta (DE3) (Novagen) and purified from cell lysates by Ni-NTA affinity chromatography. Proteins for assays were eluted by PreScission protease cleavage. Eight-histidine-tagged GFL for crystallization was eluted by 250 mM imidazole. After Ni-NTA affinity chromatography, the buffers were changed to 20 mM Tris and 1 mM EGTA (pH 8.0) on a desalting column (Hiprep 26/10; GE Healthcare). The proteins were then bound to an anion-exchange resource Q column (GE Healthcare) and washed thoroughly with 20 mM NaCl, 1 mM EGTA, and 20 mM Tris·HCl (pH 8.0), followed by 0.1 mM EGTA and 20 mM Tris·HCl (pH 8.0). GFL was eluted with 20 mM Tris·HCl and 2 mM $CaCl_2$ (pH 8.0), whereas mutants and truncates were eluted with a gradient to 1 M NaCl, 0.1 mM EGTA, and 20 mM Tris·HCl (pH 8.0). Size-exclusion chromatography (Superdex 200; GE Healthcare) was carried out in 50 mM NaCl, 0.1 mM EGTA, and 5 mM Hepes (pH 7.2). Recombinant G4–G6 was expressed and purified as described previously (12). The purity of proteins was assessed by SDS/PAGE (Figs. S1 and S2), and the activity of GFL was verified (Fig. S3).

Gelsolin–Actin Complex Preparation. Actin was purified from rabbit skeletal muscle as described previously (9). Eight-histidine-tagged human GFL in 1 mM EDTA and 25 mM Tris·HCl (pH 8.0) was incubated with 2 mM $CaCl_2$ at 4 °C for 5 min, then mixed with actin in 0.2 mM $CaCl_2$, 0.2 mM ATP, 1 mM DTT, and 2 mM Tris·HCl (pH 7.6–7.8) (buffer A) at a molar ratio of 1:2. EGTA was added to the mixture to a final concentration of 5 mM. The resulting solution was incubated at 4 °C overnight and then purified by gel filtration (Sephacryl S300; 90 × 2.5 cm; Bio-Rad) at room temperature, with elution by 1 mM EGTA, 1 mM DTT, and 10 mM Tris·HCl (pH 7.5) at a rate of 2 mL/min. The final concentration of the GFL–actin complex was 10 mg/mL, as determined by absorbance spectrophotometry (Perkin–Elmer Lambda 4B) at 280 nm by using a calculated absorption coefficient of 1.3 mL mg^{-1} cm^{-1}. The purity of GFL–actin was verified by SDS/PAGE. Two clean bands were observed at 83 kDa and 42 kDa, respectively.

Crystallization and Data Collection: Ca-Free Gelsolin. Crystals of Ca-free, eight-histidine-tagged human GFL were obtained after mixing a 20 mg/mL solution of protein with precipitant solution [15% glycerol, 1.5 M ammonium sulfate, and 100 mM Bis-Tris·HCl (pH 8.5)] at 25 °C by using the hanging-drop vapor diffusion method. The crystals were frozen in liquid nitrogen after soaking in the precipitant solution supplemented with 20% glycerol. X-ray diffraction data were collected on beamline BL13B1 on an Area Detection Systems Corporation Quantum-315 CCD detector at the National Synchrotron Research Center (Hsinchu, Taiwan). The wavelength was set to 1 Å and the data collected at 105 K. Data were indexed, scaled, and merged in HKL2000 (Table S1) (28).

G1–G3/Actin Complex. Crystals of G1–G3/actin were obtained by mixing a 10 mg/mL solution of GFL–actin complex with precipitant solution [9% PEG4000, 100 mM Ca acetate, and 100 mM sodium acetate (pH 4.6)] by using the hanging-drop vapor diffusion method. The crystals were flash frozen in liquid nitrogen after soaking in precipitant solution supplemented with 24% glycerol. Initial diffraction data from the crystals were collected to a resolution of 3.3 Å by using a Rigaku RU200 rotating anode source with OSMIC mirrors and a MAR345 image plate detector at the University of British Columbia Centre for Blood Research (Vancouver, BC, Canada). Subsequently, higher-resolution data were collected on beamline BL13B1 on the Area Detection Systems Corporation Quantum 315 CCD detector at the National Synchrotron Research Center. The wavelength was set to 1 Å and the data collected at 105 K. Data were indexed, scaled, and merged in HKL2000 (Table S1) (28). As found previously with a similar complex prepared from natural source equine plasma gelsolin and rabbit muscle actin (9), the X-ray structure from these GFL–actin crystals reveals the N-terminal half of gelsolin bound to one actin but does not

reveal the C-terminal half of gelsolin. This may indicate that proteolysis occurred during the time required for the crystals to nucleate.

Structure Solution and Refinement. Structural analysis of human Ca-free gelsolin was initiated by molecular replacement using horse Ca-free gelsolin (Protein Data Bank ID 1D0N; ref. 6) as a model. Similarly, horse G1–G3/actin (Protein Data Bank ID 1RGI; ref. 9) served as the molecular replacement template for human G1–G3/actin. Both structures contain two molecules in the asymmetric unit. Rounds of restrained refinement with TLS refinement maintaining strict noncrystallographic restraints followed by manual rebuilding resulted in the final models. MOLREP, REFMAC5, and COOT were used within the CCP4 suite of crystallographic programs (29).

Pyrene Actin Assay. Buffer F [final concentration, 50 mM KCl, 0.2 mM ATP, 2 mM $MgCl_2$, 0.5 mM DTT, 1 mM EGTA, and 50 mM Hepes (pH 7.5)] was added to 10% pyrene-labeled G actin (12 μM) in 96-well, flat-bottomed plates (Corning) and incubated for 30 min to allow the formation of F actin. Ca was then added to obtain the required free Ca concentrations. Reactions were equilibrated for 1 h before 6 μM of the respective gelsolin proteins were added. The final volume in each well was 100 μL. Fluorescence intensity was measured kinetically at wavelength 407 nm by using a Safire^2 fluorimeter (Tecan). TIRF microscopy confirmed that gelsolin is able to sever actin at this 2:1 protein ratio (1 μM actin and 0.5 μM gelsolin) (Movie S4).

Thermal Shift Assays. Ca titration gradients were formed from a Ca chloride standard (Sigma) in 80 mM Hepes, 100 mM NaCl, and 2 mM EGTA (pH 7.5). Free and total Ca levels were calculated by using WEB-MAXC (http://maxchelator.stanford.edu/). The reaction mixture, consisting of 12.5 μL of Ca-containing buffer, 5 μL of protein (final concentration, 6 μM), and 7.5 μL of 100$\times$ Sypro orange (Molecular Probes), was added to each well in 96-well PCR plates (BioRad). Plates were sealed and subjected to a temperature ramp from 20 °C to 80 °C in 0.2 °C increments in an iCycler iQ Real-Time PCR Detection System (BioRad). The transition temperature of each protein was determined as described previously (30).

ACKNOWLEDGMENTS. R.C.R. thanks the Biomedical Research Council of A*STAR for support. We thank the National Synchrotron Radiation Research Center, a national user facility supported by the National Science Council of Taiwan, Republic of China, for provision of beam time and assistance in data collection. This work was funded in part by a grant-in-aid from the Heart and Stroke Foundation of BC & Yukon (to L.D.B.). Funding for the University of British Columbia Centre for Blood Research is provided in part by grants from the Canada Foundation for Innovation, the Michael Smith Foundation for Health Research, the Howard Hughes Medical Institute, and the Canadian Institutes of Health Research. The Synchrotron Radiation Protein Crystallography Facility is supported by the National Research Program for Genomic Medicine.

1. Silacci P, et al. (2004) Gelsolin superfamily proteins: Key regulators of cellular functions. *Cell Mol Life Sci* 61:2614–2623.
2. Yin HL, Kwiatkowski DJ, Mole JE, Cole FS (1984) Structure and biosynthesis of cytoplasmic and secreted variants of gelsolin. *J Biol Chem* 259:5271–5276.
3. Kwiatkowski DJ, Mehl R, Yin HL (1988) Genomic organization and biosynthesis of secreted and cytoplasmic forms of gelsolin. *J Cell Biol* 106:375–384.
4. Way M, Weeds A (1988) Nucleotide sequence of pig plasma gelsolin. *J Mol Biol* 203:1127–1133.
5. Koepf EK, Hewitt J, Vo H, MacGillivray RTA, Burtnick LD (1998) Equus caballus gelsolin cDNA sequence and protein structural implications. *Eur J Biochem* 251:613–621.
6. Burtnick LD, et al. (1997) The crystal structure of plasma gelsolin: Implications for actin severing, capping, and nucleation. *Cell* 90:661–670.
7. Choe H, et al. (2002) The calcium activation of gelsolin: Insights from the 3 Å structure of the G4–G6/actin complex. *J Mol Biol* 324:691–702.
8. Chumnarnsilpa S, et al. (2006) Calcium ion exchange in crystalline gelsolin. *J Mol Biol* 357:773–782.
9. Burtnick LD, Urosev D, Irobi E, Narayan K, Robinson RC (2004) Structure of the N-terminal half of gelsolin bound to actin: Roles in severing, apoptosis and FAF. *EMBO J* 23:2713–2722.
10. Kazmirski SL, et al. (2002) Loss of a metal-binding site in gelsolin leads to familial amyloidosis-Finnish type. *Nat Struct Biol* 9:112–116.
11. Kolappan S, Gooch JT, Weeds AG, McLaughlin PJ (2003) Gelsolin domains 4–6 in active, actin-free conformation identifies sites of regulatory calcium ions. *J Mol Biol* 329:85–92.
12. Narayan K, et al. (2003) Activation in isolation: Exposure of the actin-binding site in the C-terminal half of gelsolin does not require actin. *FEBS Lett* 552:82–85.
13. Kothakota S, et al. (1997) Caspase-3-generated fragment of gelsolin: Effector of morphological change in apoptosis. *Science* 278:294–298.
14. Pope BJ, Maciver S, Weeds AG (1995) Localization of the calcium-sensitive actin monomer binding site in gelsolin to segment 4 and identification of calcium binding sites. *Biochemistry* 34:1583–1588.
15. Patkowski A, Seils J, Hinssen H, Dorfmuller T (1990) Size, shape parameters, and Ca^{2+}-induced conformational change of the gelsolin molecule: A dynamic light scattering study. *Biopolymers* 30:427–435.
16. Pope BJ, Gooch JT, Weeds AG (1997) Probing the effects of calcium on gelsolin. *Biochemistry* 36:15848–15855.
17. Ashish, et al. (2007) Global structure changes associated with Ca^{2+} activation of full-length human plasma gelsolin. *J Biol Chem* 282:25884–25892.
18. Kiselar JG, Janmey PA, Almo SC, Chance MR (2003) Structural analysis of gelsolin using synchrotron protein footprinting. *Mol Cell Proteomics* 2:1120–1132.
19. Kiselar JG, Janmey PA, Almo SC, Chance MR (2003) Visualizing the Ca^{2+}-dependent activation of gelsolin by using synchrotron footprinting. *Proc Natl Acad Sci USA* 100:3942–3947.
20. Maury CP (1991) Gelsolin-related amyloidosis. Identification of the amyloid protein in Finnish hereditary amyloidosis as a fragment of variant gelsolin. *J Clin Invest* 87:1195–1199.
21. Chen CD, et al. (2001) Furin initiates gelsolin familial amyloidosis in the Golgi through a defect in Ca^{2+} stabilization. *EMBO J* 20:6277–6287.
22. Page LJ, et al. (2005) Metalloendoprotease cleavage triggers gelsolin amyloidogenesis. *EMBO J* 24:4124–4132.
23. de la Chapelle A, et al. (1992) Gelsolin-derived familial amyloidosis caused by asparagine or tyrosine substitution for aspartic acid at residue 187. *Nat Genet* 2:157–160.
24. Suk JY, Zhang F, Balch WE, Linhardt RJ, Kelly JW (2006) Heparin accelerates gelsolin amyloidogenesis. *Biochemistry* 45:2234–2242.
25. Urosev D, Ma Q, Tan ALC, Robinson RC, Burtnick LD (2006) The structure of gelsolin bound to ATP. *J Mol Biol* 357:765–772.
26. Allen PG (1997) Functional consequences of disulfide bond formation in gelsolin. *FEBS Lett* 401:89–94.
27. Kurokawa H, Fujii W, Ohmi K, Sakurai T, Nonomura Y (1990) Simple and rapid purification of brevin. *Biochem Biophys Res Comm* 168:451–457.
28. Otwinowski Z, Minor W (1997) Processing of X-ray diffraction data collected in oscillation mode. *Methods Enzymol* 276:4866–4871.
29. Collaborative Computational Project, Number 4 (1994) The CCP4 suite: Programs for protein crystallography. *Acta Crystallograllogr D Biol Crystallogr* 50:760–763.
30. Pantoliano MW, et al. (2001) High-density miniaturized thermal shift assays as a general strategy for drug discovery. *J Biomol Screen* 6:429–440.